Palaeogeography, Palaeoclimatology, Palaeoecology 664 (2025) 112811

Contents lists available at ScienceDirect

Palaeogeography, Palaeoclimatology, Palaeoecology

journal homepage: www.elsevier.com/locate/palaeo

Surface and bottom water dynamics across the onset of the Messinian Salinity Crisis in the Piedmont Basin (NW Italy): Integrating micropaleontological and stable isotope evidence

A.M. Mancini [a,*], E. Nallino [b], F. Dela Pierre [b], R. Gennari [b], M. Natalicchio [b], G. Carnevale [b], G. Della Porta [c], A. Negri [a], F. Lozar [b]

[a] Department of Life and Environmental Science, Università Politecnica delle Marche, 60122 Ancona, Italy
[b] Department of Earth Sciences, Università degli Studi di Torino, 10125 Torino, Italy
[c] Department of Earth Sciences "A. Desio", Università degli Studi di Milano, 20133 Milan, Italy

ARTICLE INFO

Editor: M Elliot

Keywords:
Mediterranean
Extreme events
Deoxygenation
Calcareous nannofossils
Foraminifers
Stable isotopes

ABSTRACT

The pace and nature of paleoenvironmental dynamics leading to the Messinian Salinity Crisis (MSC) remain debated, with conflicting interpretations from the fossil and geochemical proxies.

This study focuses on two key sections in the Piedmont Basin (NW Italy), Pollenzo and Govone, representing the northernmost Mediterranean sector during the Messinian. By implementing the previously published calcareous nannofossil assemblages with new data and analyzing carbon and oxygen stable isotopes from benthic and planktic foraminifers, this research aims at understanding surface and bottom water conditions around the MSC onset (5.97 Ma).

In this gypsum-free part of the basin, calcareous nannofossil abundance remained stable for ~40 kyrs into the MSC, before disappearing, likely due to taphonomic bias. Isotopic records from the benthic foraminifer *Bolivina dilatata* suggest variations in living depth, remineralization, temperature and isotopic composition of water. Oxygen isotope data from planktic foraminifer show little variation between the 6.83–6.79 Ma and 6.05–5.99 Ma intervals, suggesting only moderate salinity and/or temperature fluctuations between the different time intervals.

These findings interpreted in the light of previous records—including organic geochemistry, fish, pollen, and dinocyst fossils pointing to salinity fluctuations between normal marine to brackish—suggest that hypersaline conditions did not characterize the early phase of the MSC in this part of the basin. These insights challenge the traditional view of widespread hypersalinity during the MSC onset, highlighting the need to integrate multiple datasets to better understand the Messinian environments in the Mediterranean Basin.

1. Introduction

The reconstruction of the Messinian environment in the Mediterranean Basin is one of the most intriguing and debated research topics in Earth Sciences, which has involved multiple disciplines, including biology, geology, chemistry, and physics (Roveri et al., 2014; Roveri et al., 2024; Agiadi et al., 2024). The onset of the Messinian Salinity Crisis (MSC; 5.97–5.33 Ma; Manzi et al., 2013), widely regarded as the most recent extreme geological event in the Mediterranean Basin, is thought to have been associated with—and potentially triggered by—the progressive reduction in water exchange with the Atlantic Ocean. This reduction followed the tectonic restriction of the paleo-Gibraltar gateways (Flecker et al., 2015; Corbí et al., 2020; Bulian et al., 2023). On the contrary, the role of climate as a major triggering mechanism for the MSC (i.e. increased evaporation over precipitation and/or cooling) was mostly discarded by analyses on the pollen record of the Messinian pre-evaporitic and evaporitic Mediterranean successions (Bertini, 2006; Bertini and Martinetto, 2011; Bertini and Menichetti, 2015; Bertini et al., 2024). The restriction of the Mediterranean Basin started well before the MSC onset, with the first evidence dating back to the Tortonian–Messinian transition (Sierro et al., 2003; Bulian et al., 2021). One of the major sedimentological expressions of such

* Corresponding author.
E-mail address: a.m.mancini@staff.univpm.it (A.M. Mancini).

https://doi.org/10.1016/j.palaeo.2025.112811
Received 8 October 2024; Received in revised form 31 January 2025; Accepted 11 February 2025
Available online 12 February 2025

restriction is represented by the deposition of organic-rich sediments (sapropels) testifying periods of water column stratification and increased residence time of bottom water (Kouwenhoven and Van der Zwaan, 2006).

In marginal Mediterranean basins, such as the Vena del Gesso (northern Apennine, N Italy) and the Sorbas (Almeria, SE Spain) basins, the onset of gypsum deposition defines the beginning of the MSC (Primary Lower Gypsum unit, PLG, 5.97–5.60 Ma; Roveri et al., 2014). The PLG unit is marked by 15–16 precession-driven lithological cycles consisting of gypsum-shale couplets (Krijgsman et al., 2001; Rohling et al., 2008; Roveri et al., 2014). However, in the Piedmont Basin, the gypsum deposition is often delayed (for up to 3 precession cycles in Pollenzo), and the lower PLG gypsum cycles laterally grade in the depocenter to organic-rich shales and limestone/marls couplets, as in the case of Govone (Dela Pierre et al., 2011; Sabino et al., 2020a).

Since the first discovery of evaporite deposits onshore and offshore (Selli, 1960; Ruggieri, 1967; Hsu, 1972), a catastrophic scenario has been suggested, which involved the almost complete desiccation of the Mediterranean Basin and the related annihilation of most of the autochthonous eukaryotes, primarily due to hypersalinity in the water column (Blanc-Valleron et al., 2002; Rouchy and Caruso, 2006). The catastrophic nature of the MSC has been questioned by several lines of evidence, first of all, by the abundance of fossil remains, which suggests a rather deep-water column and salinity fluctuations, spanning from brackish to normal marine (e.g. Landini and Sorbini, 1989; Fourtanier et al., 1991; Goubert et al., 2001; Saint Martin et al., 2001; Néraudeau et al., 2002; Carnevale et al., 2008a, 2008b; Carnevale and Schwarzhans, 2022; for more detail refer to Carnevale et al., 2019). Also, the presence of marine diatoms and low-salinity fluid inclusions in the gypsum strongly hint for the absence of hypersalinity (Natalicchio et al., 2014; Evans et al., 2015; Costanzo et al., 2019; Pellegrino et al., 2021).

This study aims to unravel the paleoceanographic changes toward and during the initial phase of the MSC in the Piedmont Basin by combining geochemical and micropaleontological data. Therefore, the bottom and surface water conditions before (6.83–6.79 Ma and 6.05–5.97 Ma) and during the PLG phase (three gypsum-free precession cycles, corresponding to 5.97–5.93 Ma) were reconstructed. The Piedmont Basin represents the northernmost Mediterranean Basin affected by the MSC and allows exploring the transition to the MSC onset across marginal (i.e. the Pollenzo section; Dela Pierre et al., 2012) and more distal (i.e. the Govone section; Sabino et al., 2020a, 2020b) sectors of the basin.

2. Material and methods

2.1. Geological setting

A sedimentary succession ranging from the Oligocene to the Messinian characterizes the Piedmont Basin. Messinian outcrops are found at the southern and northern basin margins (Fig. 1). The sedimentary succession begins with outer shelf deposits, known as the Sant'Agata Fossili Marls (SAF), which date back to the Tortonian and early Messinian (Sturani and Sampò, 1973). These deposits consist of cyclical alternations of shale and marlstone, formed under orbital forcing, primarily driven by precession (Lozar et al., 2010; Violanti et al., 2013; Natalicchio et al., 2019). At the basin margins, the SAF is overlain by sulfate evaporites of the PLG unit (Dela Pierre et al., 2011), whereas in the basin depocenter, gypsum grades into shale deposits (Irace et al., 2005). Therefore, the base of the PLG unit is diachronous and does not always coincide with the MSC onset (Fig. 1). This study focuses on the uppermost part of the SAF and the lowermost part of the PLG unit in the Pollenzo and Govone sections, which represent marginal and distal sectors of the basin, respectively (Dela Pierre et al., 2012; Sabino et al., 2020a).

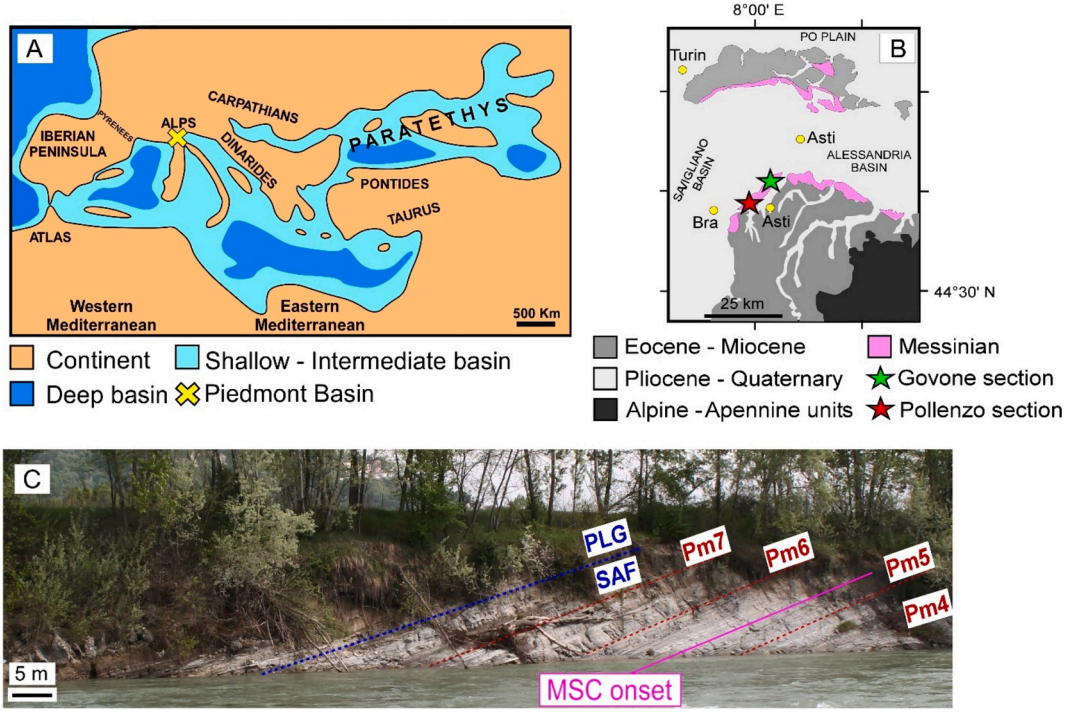

Fig. 1. Stratigraphic succession and location of the analyzed sections. A: Paleogeographic map of the Mediterranean Basin during the early Messinian (modified after Popov et al., 2006). B: Geological sketch of the Piedmont Basin (modified after Natalicchio et al., 2019). C: Landscape view of the upper part of the Pollenzo section with marked cycles (dotted red lines and labels) and geological units (dotted blue lines and labels) and the MSC onset (violet line and label) according to Lozar et al. (2010), Dela Pierre et al. (2011), Violanti et al. (2013) and Lozar et al. (2018). (For interpretation of the references to colour in this figure legend, the reader is referred to the web version of this article.)

2.2. Studied sections

2.2.1. Pollenzo

The present study focuses on the upper part of the Pollenzo section (44°41′08″N; 7°55′33″E), which was already exhaustively described in terms of stratigraphy and sedimentology (Dela Pierre et al., 2011; Dela Pierre et al., 2012; Violanti et al., 2013; Natalicchio et al., 2019). The fluctuations in the abundance of micro and nannofossils in the pre-evaporitic succession (Violanti et al., 2013; Lozar et al., 2018), along withgeochemical signatures (major and trace elements) in PLG deposits (Natalicchio et al., 2019) enabled the correlation of lithological cyclicity with Earth's orbital parameter periodicity, primarily driven by precession. The studied section is interrupted by a slump, which separates the upper seven cycles from the lower cycles. The slump is ~90 m thick and approximately spans 0.7 Ma, from 6.75 to 6.05 Ma (Lozar et al., 2010). The lower part of the studied section shows two cycles of organic-rich shale and marlstone, biostratigraphically and astronomically dated from 6.83 to 6.79 Ma (Lozar et al., 2010). The upper part of the studied section is composed of seven cycles of organic-rich shale and marlstone/carbonate (locally labeled as Pm1 – Pm7; Fig. 1) with an inferred age of 6.05–5.93 Ma (Manzi et al., 2013; Lozar et al., 2018). The organic-rich shale is olive to gray with a finely laminated texture; these deposits are irregularly interbedded with cm-thick sandy and silty layers. The marlstone is whitish/grey and bioturbated in all cycles, except in cycles Pm6 and Pm7. In these cycles, the marlstone/carbonate layers are laminated and characterized by filamentous fossils attributed to remains of sulfide-oxidizing bacteria, probably *Beggiatoa*-like (Dela Pierre et al., 2012; Natalicchio et al., 2019). Carbonate-rich (calcite, dolomite and aragonite) layers occur in the marly interbeds and represent microbially-induced authigenic carbonate precipitation (Dela Pierre et al., 2012).

The MSC onset was placed at the base of the marlstone bed of cycle Pm5, as reconstructed by integrating physical stratigraphic and biostratigraphic data (Dela Pierre et al., 2011; Lozar et al., 2018; Natalicchio et al., 2021; Gennari et al., 2024). Hence, in the studied succession the MSC onset occurs in Pm5, while cycles Pm1 to Pm4 represent the pre-MSC deposits (Fig. 1; Dela Pierre et al., 2011; Dela Pierre et al., 2012; Lozar et al., 2018; Natalicchio et al., 2021). The samples from the upper part of the section are the same as those used by Violanti et al. (2013) and Natalicchio et al. (2019), while ten additional samples were collected for the lower part.

2.2.2. Govone

The Govone section (44°48′08″N; 8°07′34″E) is representative of a more distal sector of the Piedmont Basin with respect to Pollenzo (Dela Pierre et al., 2011). A total of 44 lithological cycles were described in the Govone section (locally labeled Gm1 to Gg9) and correlated with the insolation curve (Gennari et al., 2020). The most prominent difference between the two sections is the absence of carbonate beds intercalated within the massive marlstone at Govone. Similarly to the Pollenzo section, the MSC onset does not correspond to the base of evaporites, but it is recorded in the local cycle Gm30, six precession cycles below the first gypsum bed (Gennari et al., 2020). The pre-MSC interval displays similar characteristics to Pollenzo in terms of cyclicity, with alternations of dark organic-rich laminated shale and light gray massive marlstone; however, no lithological change is observed across the MSC onset. A remarkable difference with respect to Pollenzo is the disappearance of calcareous fossils in the sedimentary record from cycle Gm28; thus, samples were collected from cycles Gm19 to Gm27, an interval spanning an inferred age of 6.20–6.02 Ma (Sabino et al., 2020a, 2020b; Gennari et al., 2020; Bertini et al., 2024). Therefore, these deposits can be utilized to extend the isotopic record of Pollenzo and extract a longer trend toward the onset of the MSC.

2.3. Calcareous nannofossils

In the present study, the dataset published by Violanti et al. (2013) and Lozar et al. (2018) is implemented by adding the analysis of 30 samples from cycles Pm4, Pm5 and Pm6. Standard smear slides were prepared and observed at 1250× with the optical microscope (Olympus BX50). At least 500 nannofossil specimens (excluding reworked specimens) were identified and counted to obtain relative abundance. The preservation of calcareous nannofossils was qualitatively assessed for each sample by considering the presence of dissolution features on the nannofossil platelets.

2.4. Carbon and oxygen stable isotopes

Carbon and oxygen stable isotopes were analyzed on planktic (*Turborotalita quinqueloba* and *Orbulina universa*) and benthic (*Bolivina dilatata*) foraminifers on the sediment residue prepared by Violanti et al. (2013) and Natalicchio et al. (2019) for the Pollenzo section, and by Gennari et al. (2020) for the Govone section. Additional ten samples were prepared for the foraminifer extraction (*O. universa*) in the lower part of the Pollenzo section, following the same procedure as in Violanti et al. (2013), Natalicchio et al. (2019) and Gennari et al. (2020). The selection of the taxa depended on their relative abundance and continuity in the analyzed sections. The picking was performed in the >125 μm fraction; however, due to the scarce abundance of the selected taxa in this size range, the 63–125 μm fraction was used for cycles Pm4-Pm7. To highlight possible inconsistency between the foraminifers picked in different size fractions, we performed isotope analyses on both size fractions in the same sample if possible. In order to avoid contamination of secondary calcite in the foraminifer inner/outer shell, which is a recurrent feature approaching the MSC onset in various sections across the Mediterranean (Sierro et al., 2003; Reghizzi et al., 2017; Mancini et al., 2020), we performed a procedure of selection and cleaning. First, a pre-selection of the best-preserved specimens was performed under optical microscope by adding a small amount of deionized water; this allowed making the shell interior more transparent, thus avoiding picking largely encrusted specimens. Successively, the picked specimens were put in the 1.4 × 2.5 cm vials, rinsed with deionized water and sonicated for ~2.5 s. The supernatant was removed, and the process was repeated at least twice. A second observation under the optical microscope was performed to roughly check the preservation and to exclude the inadequately preserved specimens. The collected specimens of all samples were further observed at the Scanning Electron Microscope (SEM) equipped with an energy-dispersive X-ray spectroscopy (EDS) to evaluate the overall effectiveness of the cleaning procedure. At the end of the cleaning procedure, 36 samples composed of ~300 μg of cleaned calcite were obtained: 35 for *B. dilatata*, 3 for *T. quinqueloba* and 11 for *O. universa*. To highlight long-term differences in $\delta^{18}O_{O.\ universa}$ toward the MSC onset, we analyzed four samples in the upper part of the section (above the slump reported in Lozar et al., 2010) and seven in the lower part, with an inferred age of 6.05–5.99 Ma and 6.83–6.79 Ma, respectively (Lozar et al., 2010). Successively, the samples were analyzed for the carbon and oxygen isotope composition using an automated carbonate preparation device (Gasbench II) and a Thermo Fisher Scientific Delta V Advantage continuous flow mass spectrometer at the University of Milan. Carbon and oxygen isotope values are expressed in the conventional delta notation calibrated to the Vienna Pee-Dee Belemnite (V-PDB) scale by the international standards IAEA 603 and NBS-18. Analytical reproducibility was better than ±0.1 ‰.

3. Results

3.1. Calcareous nannofossils

The calcareous nannofossil assemblage in the analyzed samples shows similar characteristics in terms of taxa abundance and preservation with those observed in samples previously analyzed by Violanti et al. (2013) and Lozar et al. (2018). Generally, the abundance of calcareous nannofossils is moderate in the shale and scarce in the

marlstone layers, and the preservation of the specimens spans from moderate to poor. The most abundant taxa are reticulofenestrids, with *Reticulofenestra minuta* as dominant in almost all samples, reaching 80 % (Fig. 2). *Reticulofenestra haqii* and *R. perplexa* are always present and show abundance spanning from 1.2 % to 12.2 % and from 0.9 % to 12.0 %, respectively (Fig. 2). The remaining taxa are either in low abundance (*Coccolithus pelagicus* and *R. pseudoumbilicus*), or abundant in certain samples (*Sphenolithus abies*, *Umbilicosphaera jafari*, *U. rotula*, *Helicosphaera carteri*, *Syracosphaera* sp.1, *Rhabdosphaera clavigera* and discoasterids); the remaining taxa (*S. moriformis*, *Calcidiscus leptoporus*, *Pontosphaera multipora*, *P. discopora*) are rare or extremely rare and always <1 %.

3.2. Carbon and oxygen stable isotopes

Before the cleaning and selection procedure, the foraminifers were encrusted by calcite, mainly represented by nannofossils, and by clay minerals. The cleaning procedure removed the encrustations and material filling the pores, as testified by SEM observations (Fig. S1 Supplementary Material). All the isotopic results are reported in Table 1. In the Pollenzo section, the carbon ($\delta^{13}C$) and oxygen ($\delta^{18}O$) isotope values recorded in the *B. dilatata* tests range from −5.2 to −2.1 ‰ and − 0.0 to 5.2 ‰, respectively (Fig. 3). The isotope values of *B. dilatata* recorded in the >125 μm and the 125–63 μm size fraction are similar for the $\delta^{13}C$ and $\delta^{18}O$ (differing less than 0.3 ‰; Fig. 3). A long-term trend is not observed; instead, a cyclic trend related to lithology is recorded. The $\delta^{13}C$ values of *B. dilatata* in the shale hemicycles are generally lower than those in the marlstones (Fig. 4), while the $\delta^{18}O$ values are usually lower in the marlstones (Fig. 4). *Turborotalita quinqueloba* shows $\delta^{13}C$ values ranging from −3.7 to −3.3 ‰ and $\delta^{18}O$ values from −0.1 to 4.0 ‰, while *O. universa* shows $\delta^{13}C$ values of −0.2 to 1.1 ‰ and $\delta^{18}O$ from −0.3 to 1.6 ‰ (Fig. 3). The $\delta^{18}O$ values of *O. universa* measured on the 6.83–6.79 Ma interval are similar to those of the interval 6.05–5.99 Ma, while the $\delta^{13}C$ values tend to be lower (Fig. 4). In the Govone section, the *B. dilatata* isotopic fluctuations are less marked compared to those of the Pollenzo section (Fig. 5), spanning from −3.3 to −1.8 ‰ and from 3.0 to 4.5 ‰ for $\delta^{13}C$ and $\delta^{18}O$, respectively.

4. Discussion

4.1. Surface water conditions of the MSC onset as revealed by calcareous nannofossils

At Pollenzo, calcareous nannofossils are generally abundant to common in the pre-MSC deposits (Lozar et al., 2018), and they do not show a marked reduction in abundance in the two cycles pertaining to the MSC (i.e. Pm6 and Pm7). Therefore, no major long-term changes in the upper water column are highlighted, suggesting substantially stable environmental conditions. However, the onset of the MSC is marked by a bioevent commonly identified as approximating the beginning of the crisis (Lozar et al., 2018; Lozar and Negri, 2019; Mancini et al., 2020; Gennari et al., 2024). This event was originally described by Lozar et al. (2018) and then labeled as MSC onset bioevent (Mancini et al., 2020), and it involves a transient perturbation characterized by peaks in the abundance of *S. abies* and *H. carteri*, among other species, which are indicative of a stratified water column (Perch-Nielsen, 1985; Giraudeau, 1992; Ziveri et al., 2004; Flores et al., 2005; Mejía-Molina et al., 2010). This stratification may be linked to freshening of surface waters due to increased runoff (Mancini et al., 2020). The calcareous nannofossils sharply disappear from Pm7 (Violanti et al., 2013; Lozar et al., 2018); this disappearance also involves the foraminifers record, and was recorded in several sections across the Mediterranean, although not coevally (e.g. Metochia - Greece, Sorbas - Spain, Caltanissetta - Italy, Tokhni - Cyprus; Gennari et al., 2018; Lozar et al., 2018; Mancini et al., 2022; Tzevahirtzian et al., 2023; Gennari et al., 2024). After the MSC onset bioevent, the disappearance of calcareous fossils can be related either to dissolution or adverse conditions in the water column for the proliferation of these organisms. Dissolution of aragonitic fossils or mud was widely invoked to explain either lithological bipartite cycles made of shale and carbonate or nodular limestone (Wheeley et al., 2008; Cherns and Wright, 2009; Munnecke et al., 2023). This is because aragonite tends to stabilize to the less dissolution-prone calcite, mostly in the form of micrite and microspar (Friedman, 1964; Munnecke et al., 2023). These processes mostly occur in the taphonomically active zone and the sulfate reduction-methanogenesis zones (Munnecke and

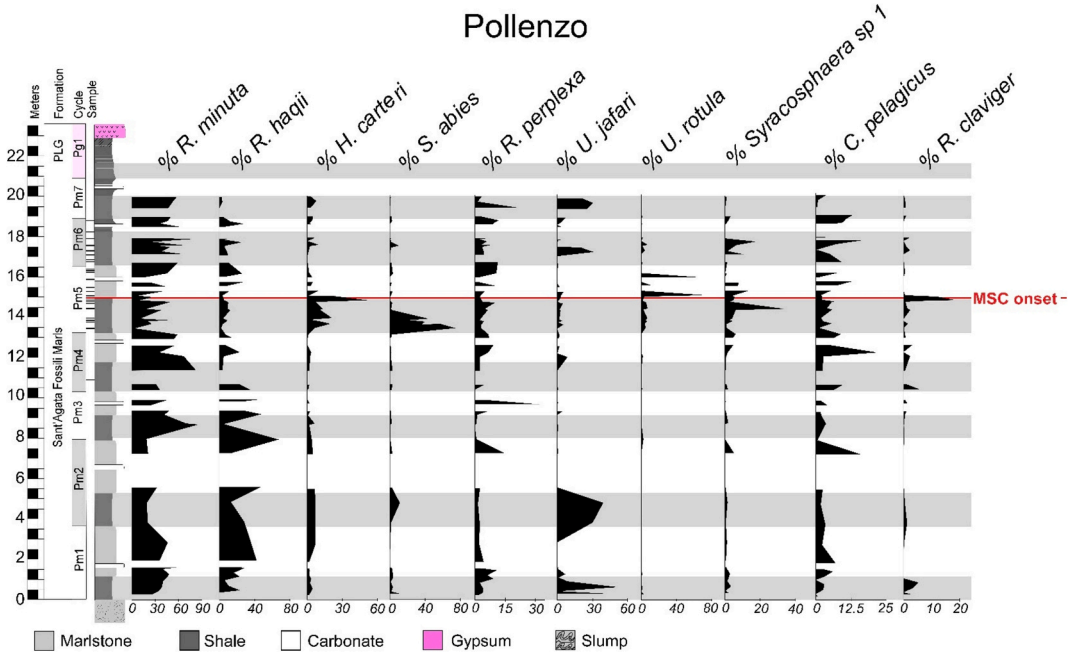

Fig. 2. Calcareous nannofossil relative abundance with the newly acquired samples marked on the left of the stratigraphic column. The identification of the MSC onset was provided by Lozar et al. (2018). From Pm4 upward the stratigraphic section is modified from Natalicchio et al. (2019). The gray rectangles correspond to the shale layers.

Table 1
Results of carbon (δ ^{13}C) and oxygen (δ^{18}O) isotope analyses of the planktic and benthic foraminifers recorded in the different sections. The depth marked with asterisk refers to the work of Lozar et al. (2010).

	Pollenzo section				
	Sample	Depth (m)	Age (Ma)	δ^{13}C (‰)	δ^{18}O (‰)
B. dilatata > 125 μm	PL 3p5	12.62	5.9906	−4.4	1.4
	E20	12.27	5.9892	−5.0	0.0
	PL 3p2	10.43	6.0103	−2.1	4.6
	PL 3p1	9.90	6.0129	−4.0	2.8
	PL 2p5	9.35	6.0102	−2.9	3.8
	EII t	9.17	6.0110	−2.9	4.1
	PL 2p3	7.96	6.0293	−2.0	5.2
	PL 2p1	6.71	6.0302	−3.7	2.7
	PL 1p6	5.54	6.0277	−3.0	3.1
	PL 1p5	4.79	6.0330	−2.9	3.3
	PL 1p3	2.81	6.0475	−2.3	4.9
	PL 1p2	1.91	6.0479	−5.2	1.7
	PL 0p5	1.50	6.0515	−4.9	3.0
	PL 0p4	1.24	6.0508	−3.6	3.6
	PM 1–50	1.07	6.0512	−3.8	4.0
	PL 0p3	0.87	6.0511	−2.5	3.6
	PL 0p2	0.60	6.0381	−2.1	3.2
B. dilatata < 125 μm	PL 4p6	15.58	5.9695	−3.5	2.6
	PL 4p1	13.00	5.9901	−2.8	2.9
	PL 3p5	12.62	5.9906	−4.5	1.0
	PL 3p1	9.90	6.0129	−4.2	2.5
	PL 0p3	0.87	6.0511	−2.6	3.4
O. universa	pl 3.4	12.07	5.9901	0.6	−0.3
	pl 2.4	8.68	6.0130	−0.1	0.6
	pl 0.3	0.87	6.0511	−0.2	1.1
	pl 0.1	0.28	6.0501	−0.1	0.3
	pc 7	14.55*	6.7967	−0.2	0.2
	pc 5	12.55*	6.8072	0.4	0.5
	cpa 16	11.45*	6.8279	1.1	1.0
	cpa 14	10.95*	6.8274	1.0	1.6
	cpa 10	10.25*	6.8262	0.7	1.3
	cpa 6a	8.70*	6.8277	0.9	1.2
	cpa 4a	7.50*	6.8295	1.0	0.3
T. quinqueloba	PM 6.4.2 63	17.59	5.9620	−3.3	−0.1
	PL 1p3 125	2.81	6.0475	−3.7	4.0
	PL 0p3 125	0.87	6.0511	−3.7	2.2
	Govone section				
B. dilatata > *125 μm*	GOVB 8p2	39.60	6.0433	−2.3	4.4
	GOV B 8p1	39.10	6.0468	−2.9	3.5
	GOV B 7p3	38.20	6.0632	−2.1	4.6
	GOV B 6p2	36.20	6.0915	−1.8	3.8
	GOV B 6p1	36.10	6.1033	−2.7	4.0
	GOV B 5p2	35.60	6.1218	−2.9	4.1
	GOV B 5p3	35.85	6.1257	−3.3	3.1
	GOV B 4p1bis	32.20	6.1429	−3.1	3.4
	GOV B 4p3	32.70	6.1549	−1.9	3.8
	GOV B 4p2	32.00	6.1601	−1.9	3.6
	GOV B 3p2	31.05	6.1776	−1.8	4.5
	GOV B 3p1	30.75	6.1783	−2.2	3.9
	GOV B 2p4	29.00	6.1903	−3.1	3.0

Samtleben, 1996; Cherns and Wright, 2009; Munnecke et al., 2023). However, it can be excluded that the lithological cyclicity of Pollenzo was related to this process because micropaleontological and geochemical evidence points to a strong orbital influence controlling the sedimentation (Lozar et al., 2010; Violanti et al., 2013; Lozar et al., 2018; Natalicchio et al., 2019). Also, it can be excluded that this process was responsible for the disappearance of nannofossils and foraminifers, because their platelets and tests are made of calcite. The disappearance of calcareous micro and nannofossils approximately at the MSC onset has traditionally been interpreted as the result of hypersaline conditions in the water column (Blanc-Valleron et al., 2002; Rouchy and Caruso, 2006; Drinia et al., 2007; Moissette et al., 2018; Zachariasse and Lourens, 2022), which are lethal to planktic foraminifers and calcareous nannoplankton. However, in Govone, the presence of genuine marine dinoflagellate cysts in the deposits overlying the disappearance of calcareous fossils suggests that the lack of biogenic calcite was not caused by hypersalinity but rather caused by a taphonomic bias due to diagenetic dissolution affecting biogenic calcite (Bertini et al., 2024). By studying the Sorbas Basin (Spain), Mancini et al. (2022) proposed that early diagenetic processes led to calcite dissolution, likely driven by the oxidation of pyrite and organic matter, which are abundant in the pre-MSC and MSC deposits (Dela Pierre et al., 2012; Natalicchio et al., 2019; Sabino et al., 2020a). The oxidation of organic matter and pyrite generates CO_2 and H^+, which are both corrosive to calcite. The transition between reducing conditions, responsible for pyrite precipitation as a byproduct of bacterial sulfate reduction, and oxygenated conditions, required for pyrite oxidation, led to increased acidity and subsequent calcite dissolution. Similarly, organic matter accumulates under reducing conditions, and its later oxidation can further contribute to calcite dissolution through CO_2 production. This mechanism of calcite dissolution around the MSC onset required high-frequency fluctuations in the oxycline, which were caused by climate-driven shifts in redox conditions in the bottom waters of a restricted basin (Mancini et al., 2022). Therefore, it is reasonable to infer that the factors leading to the disappearance of biogenic calcite observed in the Sorbas Basin were similar to those affecting the entire Mediterranean region.

However, calcite dissolution releases Ca^{2+} and HCO_3^- ions, raising the unresolved question of where these ions migrated or reacted. An intriguing hypothesis is the potential relationship between calcite dissolution and the supply of Ca^{2+} ions for gypsum deposition during the MSC (Aloisi et al., 2022).

4.2. Meaning of the Bolivina dilatata $\delta^{13}C$ and $\delta^{18}O$ signal

Reconstructing the bottom conditions preceding the onset of the MSC is essential for the understanding of the dynamics of gypsum deposition in the PLG unit, as this gypsum formed through bottom-growth processes (Lugli et al., 2010). Therefore, isotopic analyses were conducted on *Bolivina dilatata*, as it was the only benthic taxon sufficiently abundant to allow for such analysis. The stable carbon and oxygen isotope values of *B. dilatata* have not been previously studied in the Messinian deposits. Therefore, their interpretation needs a thorough examination of the ecology of this taxon, as well as a detailed review of the boundary conditions reconstructed by earlier studies in the same area (Lozar et al., 2010; Dela Pierre et al., 2012; Violanti et al., 2013; Lozar et al., 2018; Natalicchio et al., 2019; Sabino et al., 2020a; Bertini et al., 2024). The large variation recorded in both C and O isotopes (Δ up to 3.3 ‰ and 5.2 ‰, respectively; Fig. 4) cannot be explained by dimorphic (i.e. megalospheric vs microspheric) variation of the taxon, which is usually small in the species of the genus *Bolivina* (on average < 0.15 ‰; Douglas and Staines-Urias, 2007). Similarly, also the ontogenetic effect on isotopic results (e.g. Schmiedl et al., 2004) can be discarded as we performed the analysis on different size fractions (125–63 μm and > 125 μm; Fig. 3) with very similar results (Δ < 0.3 ‰). The following subsections examine the environmental and ecological conditions that contributed to the higher $\delta^{13}C_{B.\ dilatata}$ values observed in the shale hemicycles, as well as the lower values found in the marlstones (Fig. 4).

4.2.1. Bolivina dilatata $\delta^{13}C$

The genus *Bolivina*, one of the most abundant in the studied material, is a shallow infaunal benthic foraminifer generally confined to the upper two centimeters of sediment (Barmawidjaja et al., 1992; Murray, 2006). It is a eutrophic taxon, capable of thriving in oxygen-deficient conditions (Murray, 2006; Glock et al., 2019; Glock, 2023) and as an infaunal benthic foraminifer, it can move vertically in the sediment following oxygen and food availability (TROX model; Jorissen et al., 1995). According to this model, oligotrophic regimes can inhibit the benthic infaunal foraminifer proliferation; while in eutrophic regimes, infaunal foraminifers are not limited by food availability and can migrate upward vertically in conditions of oxygen depletion (Jorissen et al., 1995), exploiting the surface and shallow infaunal niche.

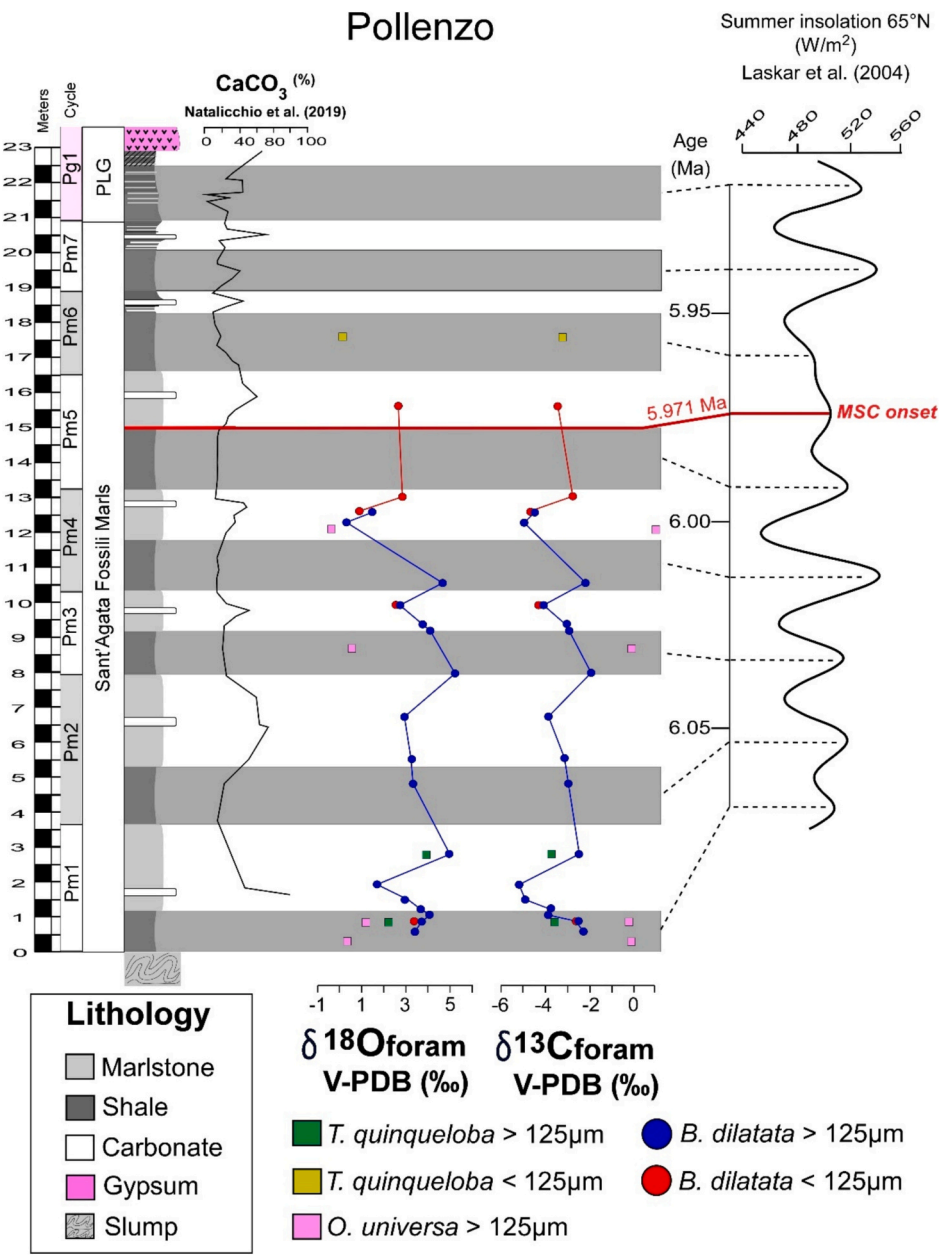

Fig. 3. Stable isotope record of planktic (*T. quinqueloba* and *O. universa*) and benthic (*B. dilatata*) foraminifers recorded in the Pollenzo section with correlation to the insolation curve (Laskar et al., 2004). $CaCO_3$ content (Natalicchio et al., 2019) is shown on the left.

In the studied case, the calcareous microfossil assemblage shows high abundances of *R. minuta* among calcareous nannofossils, *T. quinqueloba* among planktic foraminifers and of bolivinids and buliminids among the benthic assemblage, all indicative of high availability of trophic resources (Sierro et al., 2003; Violanti et al., 2013). This suggests that in this case, the vertical infaunal migration of *Bolivina* was related to bottom oxygen content.

For interpreting the data, it is important to consider the isotopic pattern of Dissolved Inorganic Carbon (DIC) in surface, bottom, and pore waters. Surface waters exhibit higher δ^{13}C-DIC values compared to bottom waters, which, in turn, are higher than those in pore waters. This gradient is driven by the release of ^{13}C-depleted CO_2 during the decomposition of organic matter in the water column and sediment pore waters (McCorkle et al., 1985; Fontanier et al., 2017). Furthermore, pore water is characterized by a gradient of the $\delta^{13}C_{DIC}$, which decreases with depth in the sediment (McCorkle et al., 1985; Fontanier et al., 2017). This gradient is especially exacerbated in eutrophic settings in relation to the organic carbon abundance (Fontanier et al., 2017; Fig. 6). Consequently, vertical migrations of benthic foraminifers within the sediment can result in different isotopic incorporation due to the DIC gradient. A previous study (Sabino et al., 2021) on Thaumarchaeota lipids from the Pollenzo and Govone sections revealed that the vertical δ^{13}C gradient of DIC between surface and bottom waters intensified at the onset of the MSC, driven by increased continental runoff and the resulting water column stratification. Furthermore, sedimentological, geochemical, and micropaleontological data suggest that the cyclical deposition of shales was linked to periods of anoxic conditions, driven by water column stratification and increased organic matter export due to enhanced continental runoff (Violanti et al., 2013; Natalicchio et al., 2019). Under these conditions, we hypothesize that *B. dilatata* migrated upward within the sediment, reflecting bottom water conditions rather than pore water. This shift resulted in higher δ^{13}C values, as observed in *B. dilatata* within the shale (Figs. 4 and 6). Conversely, intense burrowing characterizing the homogenous marlstone is indicative of a

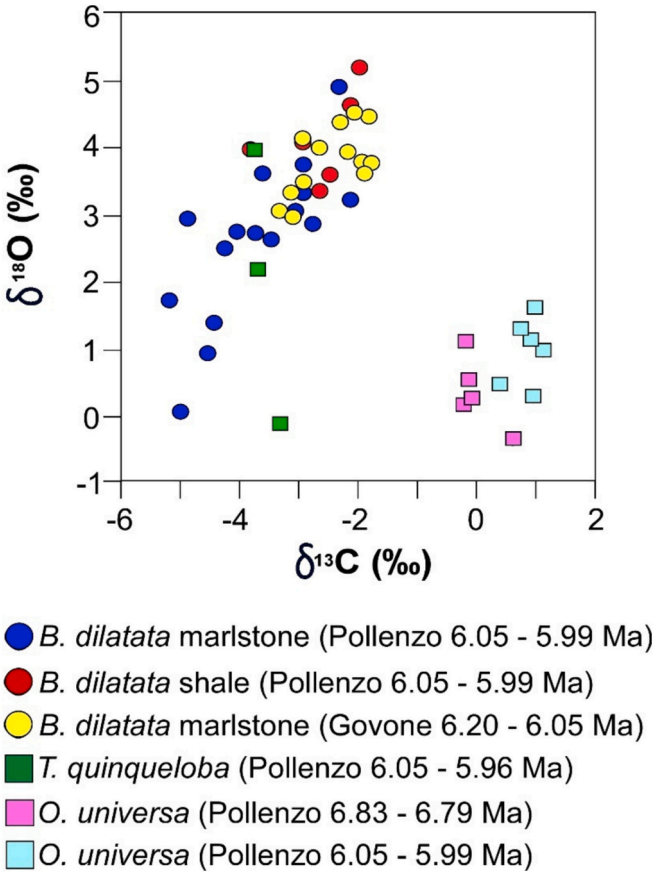

Fig. 4. Scatter plots of the stable isotope values of planktic and benthic foraminifers in the analyzed sections.

relatively well-oxygenated environment, which promoted the downward migration of *B. dilatata* and a consequent decrease of the $\delta^{13}C_{B.\ dilatata}$ (up to −5.2 ‰; Fig. 6). In addition, the high abundance of eutrophic taxa, such as *T. quinqueloba*, along with benthic species like *Bolivina* spp. and *Bulimina* spp., likely indicates a more productive regime during marlstone deposition compared to the shale. The reduced organic carbon burial during marlstone deposition further supports the presence of a well-oxygenated environment, likely driven by strong water column mixing. Additional factors influencing the $\delta^{13}C_{B.\ dilatata}$ are the pattern of organic matter remineralization in the water column, which mostly controls the ^{13}C-depleted CO_2 release. Anoxic conditions in the water column and on the seafloor, which occurred during the deposition of the shale, can slow down the remineralization of organic carbon, reducing the release of ^{13}C-depleted CO_2 (Fig. 6). In this context, the progressively higher $\delta^{13}C_{B.\ dilatata}$ values in the shales suggest declining surface productivity and lower remineralization rates during periods of water column stratification and anoxic conditions. In contrast, during marl deposition, increased water column mixing enhanced both organic carbon export and oxygen levels on the seafloor, allowing *Bolivina* to inhabit deeper sediment layers where they incorporated the lighter ^{12}C from efficiently remineralized pore water (Fig. 6).

4.2.2. *Bolivina dilatata* $\delta^{18}O$

The $\delta^{18}O$ values of benthic foraminifers reflect the bottom and/or pore water temperature and the $\delta^{18}O$ of seawater, which varies as a function of the continental ice volume and precipitation/evaporation pattern (e.g. Polyak et al., 2003; Murray, 2006). The $\delta^{18}O_{B.\ dilatata}$ shows on average higher values in the shale compared to the marlstone (Figs. 3 and 4), suggesting a colder and/or saltier bottom during the deposition of the shale compared to the homogenous marlstone. This can be explained by the vertical stratification of the water column during shale deposition, probably caused by a strong and permanent pycnocline (Fig. 6). Indeed, during insolation maxima, the continental runoff was higher. The resulting density stratification of the water column and the absence of mixing with the upper water masses could have trapped higher salinity water at the bottom of the basin (Fig. 6). Despite this, the benthic foraminifer *B. dilatata* is usually associated with high nutrient/low oxygen regime, thriving in oceanic salinity waters (Murray, 2006); therefore, it is not associated with hypersalinity. The long-term record of benthic foraminifer $\delta^{18}O$, as measured on *Planulina ariminensis* in the Ain el Beida section (NW Morocco), exhibits moderate fluctuations, typically not exceeding ~0.8 ‰ in coeval deposits (0.4–1.2 ‰; Van der Laan et al., 2005). Similarly, Bulian et al. (2023) observed fluctuations in the $\delta^{18}O$ values of *Cibicidoides pachyderma* within the same range (0.4–1.4 ‰) when studying the Montemayor section. These sites are on the Atlantic side, and document variations associated with oceanic regimes. Similarly, in the Gavdos section (Greece, Eastern Mediterranean) approaching the MSC onset, the $\delta^{18}O$ of *Bulimina aculeata* showed less marked fluctuation (Zachariasse and Lourens, 2022) compared to Pollenzo. Therefore, we infer that the pronounced fluctuation $\delta^{18}O_{B.\ dilatata}$ compared to the other coeval record of $\delta^{18}O_{Benthic}$ on the Atlantic side and in the Eastern Mediterranean is the result of a strongly fluctuating environment, probably driven by variations in freshwater input and evaporation rate in this part of the Mediterranean Basin.

4.3. The $\delta^{18}O$ stable isotope signal of *O. universa* and *T. quinqueloba*

The $\delta^{18}O$ values of *O. universa* measured on the 6.83–6.79 Ma interval are similar to those of the interval 6.05–5.99 Ma and, despite the low resolution, *T. quinqueloba* shows lower $\delta^{18}O$ values during the MSC onset (Figs. 3 and 4). The $\delta^{18}O$ of the calcite of these two taxa should reflect the control of temperature on the isotopic fractionation and the $\delta^{18}O$ of seawater in which they calcify. Typically, the modern ocean experiences a wide range of Sea Surface Temperature (SST) variations, which, in contrast to $\delta^{18}O$ of seawater, means that the $\delta^{18}O$ values of planktic foraminifers primarily reflect changes in SST (Schiebel and Hemleben, 2017). However, this is not the case for the Messinian, especially approaching the MSC onset, when variations of salinity are consistently suggested by paleontological contents (Sierro et al., 2003; Lozar et al., 2018; Mancini et al., 2020; Bertini et al., 2024). To exclude the interference of the vital effect of the different taxa (e.g. Martínez-Botí et al., 2011), we consider *O. universa* and *T. quinqueloba* isotopic trends separately. Nevertheless, to better constrain the meaning of the $\delta^{18}O$ shift of these taxa, it is imperative to highlight their ecological preferences. *Turborotalita quinqueloba* and *O. universa* are regarded to be indicative of different environmental conditions. *Turborotalita quinqueloba* is one of the most abundant taxa in the modern oceans, and its distribution mostly follows food availability in cold waters (Hemleben et al., 1989; Sierro et al., 2003; Schiebel and Hemleben, 2017; Azibeiro et al., 2023); conversely, *O. universa* occurs in a wide range of temperature and salinity and is abundant in tropical to temperate waters (Chapman, 2010; Schiebel and Hemleben, 2017). During the Messinian, these two taxa appear to show opposite trend, with *O. universa* usually dominating the assemblages during insolation maxima, and *T. quinqueloba* being abundant during insolation minima (Sierro et al., 2003; Gennari et al., 2024).

To disentangle the effects of the SST on the $\delta^{18}O$ to achieve qualitative variation in the $\delta^{18}O_{seawater}$, which is considered a salinity indicator (Kallel et al., 1997; Vasiliev et al., 2019; Kontakiotis et al., 2022; Pilade et al., 2023), we interpret our records in the light of qualitative temperature and salinity evidence reported by previous studies in the Piedmont Basin (Fig. 7). Since strong SST fluctuations were not recorded across the MSC onset (Bertini et al., 2024) and are not regarded as the main factor triggering the MSC, it can be reasonably inferred that the variation in the oxygen isotopic composition of the calcite was mainly

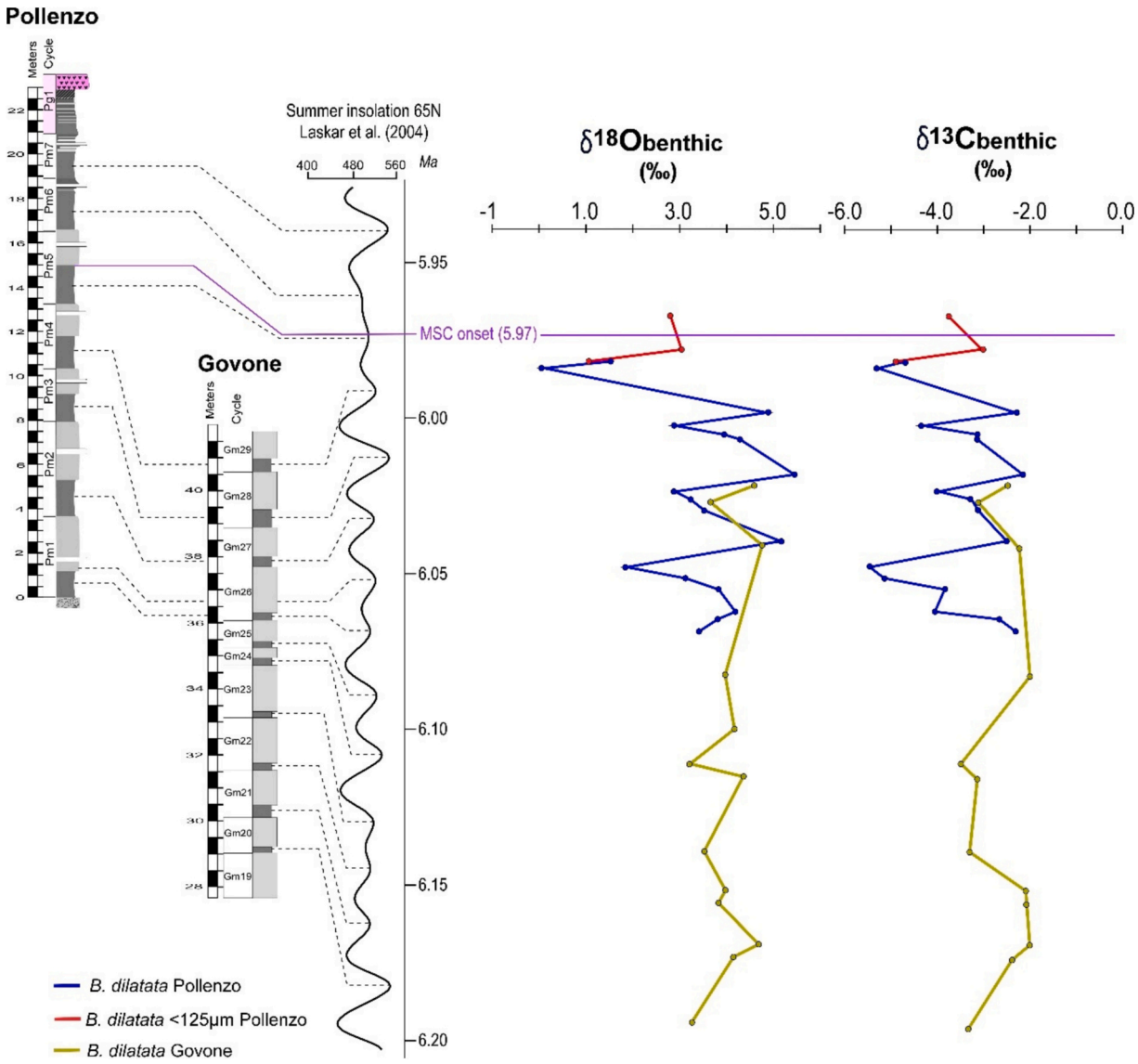

Fig. 5. The studied Pollenzo and Govone sections correlated with the variation in summer insolation (according to Laskar et al., 2004) and the combined $\delta^{13}C$ and $\delta^{18}O$ record on benthic foraminifers.

related to $\delta^{18}O_{seawater}$, hence to salinity variations.

The $\delta^{18}O_{O.\ universa}$ remained rather uniform between 6.83 and 6.79 Ma and between 6.05 and 5.99 Ma (Fig. 4), suggesting no marked changes in salinity during the season of the proliferation of this taxon before and approaching the MSC onset. This evidence points to normal marine Sea Surface Salinity (SSS) during the season of *O. universa* proliferation, which nowadays shows higher abundances during the end of the summer (Pujol and Grazzini, 1995; Chapman, 2010). During this season, it is reasonable to infer that the evaporation exceeded the precipitation, thus increasing the SSS from brackish to marine. Brackish waters are not tolerated by planktic foraminifers (Schiebel and Hemleben, 2017), thus brackish conditions during certain seasons can also explain the rather scarce abundance of planktic foraminifers (Violanti et al., 2013; Gennari et al., 2020) toward the MSC onset. Although scarce, the $\delta^{18}O_{T.\ quinqueloba}$ datapoints extended into the first precession cycle of the MSC, which is the first isotopic record of foraminiferal calcite isotope during the MSC, therefore carrying strong relevance. It can be excluded that the $\delta^{18}O_{T.\ quinqueloba}$ variation is related to the diagenetic effect that precipitated secondary calcite in the foraminifers, because the tests did not show encrustations after the cleaning procedure. Therefore, the collected $\delta^{18}O_{T.\ quinqueloba}$ datapoints span 4.2–2.3 ‰ down to −0.1 ‰, likely suggesting a salinity decrease and/or warmer conditions after the MSC onset (Fig. 3).

Other features coming from a different set of evidence suggesting low to normal salinity in the Piedmont Basin are:

i. Terrestrial lipid biomarkers suggest an increase in freshwater input across the MSC onset, which resulted in a strongly stratified water column (Natalicchio et al., 2019; Sabino et al., 2020a; Sabino et al., 2020b).
ii. The fish assemblage in the pre-MSC interval is diverse and rather abundant in diatomites and sapropelitic shales (Carnevale et al., 2019) and represented by both neritic and oceanic taxa. During the first phase of the MSC, the fish assemblage is also abundant, and from an ecological point of view, it reflects marine (e.g., *Lepidopus* spp., *Lichia* aff. *Amia* [Linnaeus, 1758]), and estuarine (e.g. *Alosa crassa* Sauvage, 1873, *Atherina* spp. [Gaudant, 1978], *Gobius* spp.) environments, despite freshwater (e.g. *Oreochromis lorenzoi* Carnevale et al., 2003) and lagoonal (e.g. *Aphanius crassicaudus*) (e.g., Sturani, 1973; Cavallo and Gaudant, 1987; Landini and Sorbini, 1989; Carnevale et al., 2003; Carnevale et al., 2008a, 2008b; Carnevale et al., 2019) taxa can be locally

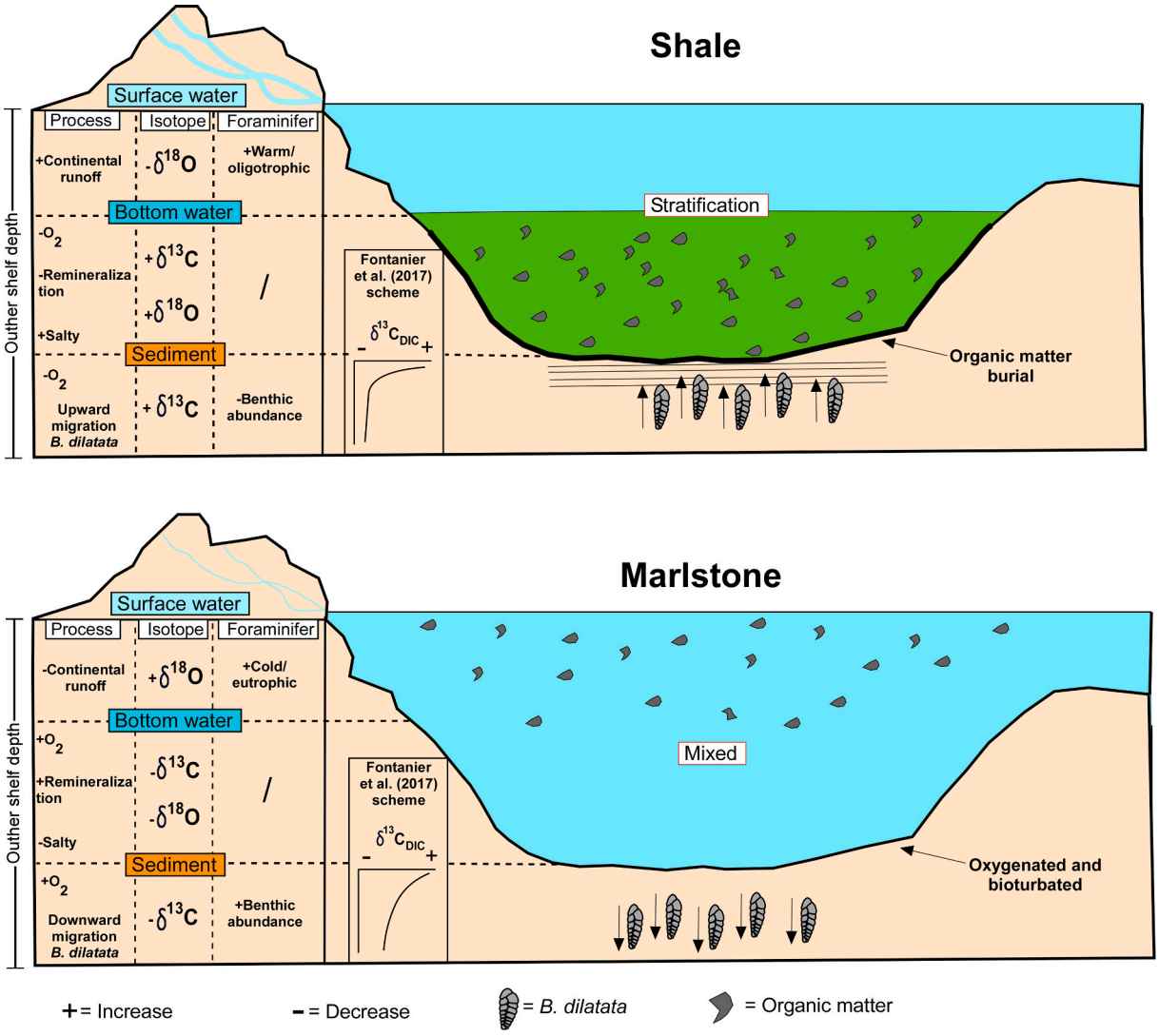

Fig. 6. Conceptual model explaining the $\delta^{18}O$ and $\delta^{13}C$ variations of *B. dilatata* in the analyzed section for the shale and marlstone. The left panel displays the processes, with the associated isotopic shifts, and key characteristics of the main foraminiferal assemblages for surface and bottom water, as well as sediment. The symbols "+" and "-"refer to increase and decrease, respectively. The scheme of the $\delta^{13}C_{DIC}$ in the sediment pore water reconstructed by Fontanier et al. (2017) is shown in the central panel.

Low salinity/absence of hypersalinity		
Evidence	**Rationale**	**Reference**
Calcareous nannofossils	Approximately at the MSC onset, peaks in abundance of low salinity tolerants and stratification indicator taxa (MSC onset bioevent)	Mancini et al. (2020)
Biomarkers	Increase in river-transported terrestrial molecular fossils	Natalicchio et al. (2019); Sabino et al. (2020a); Sabino et al., (2020b)
Fish	Presence of marine to freshwater and brackish taxa	Carnevale et al. (2019) and references theirein
Dinocysts	Presence of low salinity and absence of high salinity taxa	Bertini et al. (2024)
Foraminiferal $\delta^{18}O$	No tendency toward higher value	Present study

Fig. 7. Evidence claiming brackish and/or normal salinity waters approaching the MSC onset in the Piedmont Basin.

abundant. Collectively, fish body fossils may suggest that the transition to the MSC onset was probably characterized by salinity fluctuations, but always below the mean oceanic salinity range, thereby contrasting with hypersalinity in the water column (e.g. Carnevale and Schwarzhans, 2022).

iii. The dinocyst assemblage in the Govone section suggests a significant freshwater input influence from 6.04 Ma, attested by peaks in abundance of *Selenopemphix brevispinosa*, which is considered an inner neritic taxon indicative of reduced salinity. This is also corroborated by the disappearance at the same time of high-salinity taxa (e.g. *Operculodinium israelianum*) (Bertini et al., 2024). Also, the quite regular presence of *Tectatodinium pellitum* across and after the MSC onset, suggests relatively warm conditions, between 14.4 and 29.5 °C, and marine to brackish conditions in terms of SSS (21.9–39.2 ‰; Zonneveld and Pospelova, 2015; Bertini et al., 2024).

Overall, all these data suggest high salinity fluctuation toward the MSC, but this fluctuation was likely to range from normal marine to brackish, therefore it seems to exclude hypersalinity (Fig. 7), which agrees with the deposition of "low salinity gypsum" during the MSC (Aloisi et al., 2022; Guibourdenche et al., 2022). A long-term reduction in salinity (from ~47 to ~38 ‰) was also recorded by combining foraminiferal $\delta^{18}O$ and alkenone records in the Kalamaki and Agios Myron sections (Greece) (Vasiliev et al., 2019; Kontakiotis et al., 2022). It can be inferred that the low-salinity water at the onset of the MSC was likely caused by restricted water exchange with the Atlantic. This restriction heightened the Mediterranean sensitivity to continental runoff, which was notably high during the Messinian (Gladstone et al., 2007).

5. Conclusions

The first record of foraminifer carbon and oxygen stable isotopes in the Piedmont Basin and the refinement of calcareous nannofossil abundance toward and across the MSC onset provides valuable information about the paleoenvironmental conditions characterizing the surface and bottom waters. Calcareous nannofossils are present in the deposits of the first 40 kyrs of the MSC; their disappearance from the fossil record is attributed to a taphonomic bias affecting biogenic calcite and not to hypersalinity. By coupling previous paleontological, geochemical and sedimentological observations carried out on the Piedmont Basin, for the first time we constrained the $\delta^{18}O$ and $\delta^{13}C$ measured on *B. dilatata*, a shallow benthic infaunal foraminifer. The fluctuations characterizing the $\delta^{13}C_{B.\ dilatata}$ reflect a combination of vertical movement within the sediment and organic matter burial/remineralization pattern in the bottom and pore waters. Moreover, by combining the stable isotope results from planktic foraminifers with previous evidence we delineated the surface water conditions approaching and during the early phase of the MSC. Our reconstruction suggests the absence of hypersalinity throughout the analyzed interval; instead, all the collected evidence points to salinity fluctuations from normal marine to brackish in the Piedmont Basin. These findings are challenging the prevailing assumption of hypersaline conditions during the early MSC, highlighting the need for a paradigm shift in understanding this critical event.

CRediT authorship contribution statement

A.M. Mancini: Writing – review & editing, Writing – original draft, Visualization, Validation, Supervision, Project administration, Methodology, Investigation, Funding acquisition, Formal analysis, Data curation, Conceptualization. **E. Nallino:** Writing – review & editing, Methodology, Formal analysis, Data curation. **F. Dela Pierre:** Writing – review & editing, Validation, Investigation, Conceptualization. **R. Gennari:** Writing – review & editing, Validation, Supervision, Formal analysis, Data curation. **M. Natalicchio:** Writing – review & editing, Validation, Supervision, Methodology, Data curation. **G. Carnevale:** Writing – review & editing, Validation, Supervision, Methodology. **G. Della Porta:** Writing – review & editing, Validation, Supervision, Methodology, Formal analysis, Data curation. **A. Negri:** Writing – review & editing, Validation, Methodology, Data curation. **F. Lozar:** Writing – review & editing, Validation, Supervision, Methodology, Data curation, Conceptualization.

Declaration of competing interest

Alan Maria Mancini reports financial support was provided by ECORD-IODP Italia. If there are other authors, they declare that they have no known competing financial interests or personal relationships that could have appeared to influence the work reported in this paper.

Acknowledgment

This research was funded through MUR for ECORD-IODP Italia to A. M. M. within the project "Exploring Deoxygenation Dynamics in a Warming Climate: Insights from Oxygen-Starved Conditions in the geological record". We warmly thank two anonymous reviewers and the journal Editor for their useful and detailed suggestions.

Appendix A. Supplementary data

Supplementary data to this article can be found online at https://doi.org/10.1016/j.palaeo.2025.112811.

Data availability

Data will be made available on request.

References

Agiadi, K., Hohmann, N., Gliozzi, E., Thivaiou, D., Bosellini, F.R., Taviani, M., Bianucci, G., Collareta, A., Londeix, L., Faranda, C., et al., 2024. The marine biodiversity impact of the Late Miocene Mediterranean salinity crisis. Science 385, 986–991.

Aloisi, G., Guibourdenche, L., Natalicchio, M., Caruso, A., Haffert, L., El Kilany, A., Dela Pierre, F., 2022. The geochemical riddle of "low-salinity gypsum" deposits. Geochim. Cosmochim. Acta 327, 247–275.

Azibeiro, L.A., Kučera, M., Jonkers, L., Cloke-Hayes, A., Sierro, F.J., 2023. Nutrients and hydrography explain the composition of recent Mediterranean planktonic foraminiferal assemblages. Mar. Micropaleontol. 179, 102201.

Barmawidjaja, D.M., Jorissen, F.J., Puškarić, S., Van der Zwaan, G.J., 1992. Microhabitat selection by benthic foraminifera in the northern Adriatic Sea. J. Foraminifer. Res. 22 (4), 297–317.

Bertini, A., 2006. The Northern Apennines palynological record as a contribute for the reconstruction of the Messinian palaeoenvironments. Sediment. Geol. 188, 235–258.

Bertini, A., Martinetto, E., 2011. Reconstruction of vegetation transects for the Messinian–Piacenzian of Italy by means of comparative analysis of pollen, leaf and carpological records. Palaeogeography, Palaeoclimatology, Palaeoecology 304 (3–4), 230–246.

Bertini, A., Menichetti, E., 2015. Palaeoclimate and palaeoenvironments in Central Mediterranean during the last 1.6 Ma before the onset of the Messinian Salinity Crisis: a case study from the Northern Apennine foredeep basin. Rev. Palaeobot. Palynol. 218, 106–116.

Bertini, A., Niccolini, G., Gennari, R., Lozar, F., Menichetti, E., Natalicchio, M., Dela Pierre, F., 2024. Terrestrial and marine dynamics on the brink of the Messinian salinity crisis: a wet scenario from the northern Mediterranean. Global Planet. Change 104362.

Blanc-Valleron, M.M., Pierre, C., Caulet, J.P., Caruso, A., Rouchy, J.M., Cespuglio, G., Di Stefano, E., 2002. Sedimentary, stable isotope and micropaleontological records of paleoceanographic change in the Messinian Tripoli Formation (Sicily, Italy). Palaeogeography, Palaeoclimatology, Palaeoecology 185 (3–4), 255–286.

Bulian, F., Sierro, F.J., Ledesma, S., Jiménez-Espejo, F.J., Bassetti, M.A., 2021. Messinian West Alboran Sea record in the proximity of Gibraltar: early signs of Atlantic-Mediterranean gateway restriction. Mar. Geol. 434, 106430.

Bulian, F., Jiménez-Espejo, F.J., Andersen, N., Larrasoaña, J.C., Sierro, F.J., 2023. Mediterranean water in the Atlantic Iberian margin reveals early isolation events during the Messinian Salinity Crisis. Global Planet. Change 231, 104297.

Carnevale, G., Schwarzhans, W., 2022. Marine life in the Mediterranean during the Messinian Salinity Crisis: a paleoichthyological perspective. Rivista Italiana di Paleontologia e Stratigrafia 128, 283–324.

Carnevale, G., Caputo, D., Landini, W., 2008a. A leerfish (Teleostei, Carangidae) from the Messinian evaporite succession of the Vena del Gesso basin (Romagna Apennines,

Italy): palaeogeographical and palaeoecological implications. Bollettino della Società Paleontologica Italiana 47 (2), 169–176.
Carnevale, G., Longinelli, A., Caputo, D., Barbieri, M., Landini, W., 2008b. Did the Mediterranean marine reflooding precede the Mio–Pliocene boundary? Paleontological and geochemical evidence from upper Messinian sequences of Tuscany, Italy. Palaeogeography, Palaeoclimatology, Palaeoecology 257 (1–2), 81–105.
Carnevale, G., Gennari, R., Lozar, F., Natalicchio, M., Pellegrino, L., Dela Pierre, F., 2019. Living in a deep desiccated Mediterranean Sea: an overview of the Italian fossil record of the Messinian salinity crisis. Bollettino della Società Paleontologica Italiana 58, 109–140.
Carnevale, G., Sorbini, C., Landini, W., 2003. Oreochromis lorenzoi, a new species of tilapiine cichlid from the late Miocene of central Italy. J. Vertebr. Paleontol. 23 (3), 508–516.
Cavallo, O., Gaudant, J., 1987. Observations complémentaires sur l'Ichthyofaune des marnes messiniennes de Cherasco (Piémont): Implications géodynamiques. Bollettino della Società Paleontologica Italiana 26 (1–2), 177–198.
Chapman, M.R., 2010. Seasonal production patterns of planktonic foraminifera in the NE Atlantic Ocean: Implications for paleotemperature and hydrographic reconstructions. Paleoceanography 25 (1).
Cherns, L., Wright, V.P., 2009. Quantifying the impacts of early diagenetic aragonite dissolution on the fossil record. Palaios 24 (11), 756–771.
Corbí, H., Soria, J.M., Giannetti, A., Yébenes, A., 2020. The step-by-step restriction of the Mediterranean (start, amplification, and consolidation phases) preceding the Messinian Salinity Crisis (climax phase) in the Bajo Segura basin. Geo-Mar. Lett. 40, 341–361.
Costanzo, A., Cipriani, M., Feely, M., Cianflone, G., Dominici, R., 2019. Messinian twinned selenite from the Catanzaro Trough, Calabria, Southern Italy: field, petrographic and fluid inclusion perspectives. Carbonates Evaporites 34, 743–756.
Dela Pierre, F., Bernardi, E., Cavagna, S., Clari, P., Gennari, R., Irace, A., Violanti, D., 2011. The record of the Messinian salinity crisis in the Tertiary Piedmont Basin (NW Italy): the Alba section revisited. Palaeogeogr. Palaeoclimatol. Palaeoecol. 310 (3–4), 238–255.
Dela Pierre, F., Clari, P., Bernardi, E., Natalicchio, M., Costa, E., Cavagna, S., Violanti, D., 2012. Messinian carbonate-rich beds of the Tertiary Piedmont Basin (NW Italy): microbially-mediated products straddling the onset of the salinity crisis. Palaeogeography, Palaeoclimatology, Palaeoecology 344, 78–93.
Douglas, R., Staines-Urias, F., 2007. Dimorphism, shell Mg/Ca ratios and stable isotope content in species of Bolivina (benthic foraminifera) in the Gulf of California, Mexico. The Journal of Foraminiferal Research 37 (3), 189–203.
Drinia, H., Antonarakou, A., Tsaparas, N., Kontakiotis, G., 2007. Palaeoenvironmental conditions preceding the Messinian Salinity Crisis: a case study from Gavdos Island. Geobios 40 (3), 251–265.
Evans, N.P., Turchyn, A.V., Gázquez, F., Bontognali, T.R., Chapman, H.J., Hodell, D.A., 2015. Coupled measurements of $\delta^{18}O$ and δD of hydration water and salinity of fluid inclusions in gypsum from the Messinian Yesares Member, Sorbas Basin (SE Spain). Earth Planet. Sci. Lett. 430, 499–510.
Flecker, R., Krijgsman, W., Capella, W., de Castro Martíns, C., Dmitrieva, E., Mayser, J.P., et al., 2015. Evolution of the Late Miocene Mediterranean–Atlantic gateways and their impact on regional and global environmental change.
Flores, J.A., Sierro, F.J., Filippelli, G.M., Bárcena, M.Á., Pérez-Folgado, M., Vázquez, A., Utrilla, R., 2005. Surface water dynamics and phytoplankton communities during deposition of cyclic late Messinian sapropel sequences in the western Mediterranean. Marine Micropaleontology 56 (1–2), 50–79.
Fontanier, C., Sakai, S., Toyofuku, T., Garnier, E., Brandily, C., Eugene, T., Deflandre, B., 2017. Stable isotopes in deep-sea living (stained) foraminifera from the Mozambique Channel (eastern Africa): multispecies signatures and paleoenvironmental application. J. Oceanogr. 73, 259–275.
Fourtanier, E., Gaudant, J., Cavallo, O., 1991. La diatomite de Castagnito (Piémont): une nouvelle preuve de l'existence d'oscillations modérées du niveau marin pendant le Messinien évaporitique. Bollettino della Società Paleontologica Italiana. 30 (1), 79–95.
Friedman, G.M., 1964. Early diagenesis and lithification in carbonate sediments. J. Sediment. Res. 34 (4), 777–813.
Gaudant, J., 1978. L'ichthyofaune des marnes messiniennes des environs de Gabbro (Toscane, Italie): Signification paleoecologique. Geobios 11 (6), 905–911.
Gennari, R., Lozar, F., Natalicchio, M., Zanella, E., Carnevale, G., Dela Pierre, F., 2020. Chronology of the Messinian events in the northernmost part of the Mediterranean: the Govone section (Piedmont Basin, NW Italy). Rivista Italiana di Paleontologia e Stratigrafia 126 (2), 541–560.
Gennari, R., Lozar, F., Turco, E., Dela Pierre, F., Lugli, S., Manzi, V., Taviani, M., 2018. Integrated stratigraphy and paleoceanographic evolution of the pre-evaporitic phase of the Messinian salinity crisis in the Eastern Mediterranean as recorded in the Tokhni section (Cyprus island). Newsletters on Stratigraphy 51 (1), 33–55.
Gennari, R., Lugli, S., Manzi, V., Persico, D., Reghizzi, M., Roveri, M., 2024. Stress precursors of the Messinian salinity crisis as recorded by calcareous plankton and geochemistry in the Eastern Mediterranean: the Upper Metochia section of the Gavdos Island (Greece). Palaeogeography, Palaeoclimatology, Palaeoecology 636, 111970.
Giraudeau, J., 1992. Distribution of recent nannofossils beneath the Benguela system: southwest African continental margin. Mar. Geol. 108 (2), 219–237.
Gladstone, R., Flecker, R., Valdes, P., Lunt, D., Markwick, P., 2007. The Mediterranean hydrologic budget from a Late Miocene global climate simulation. Palaeogeogr. Palaeoclimatol. Palaeoecol. 251 (2), 254–267.
Glock, N., 2023. Benthic foraminifera and gromiids from oxygen-depleted environments–survival strategies, biogeochemistry and trophic interactions. Biogeosciences 20 (16), 3423–3447.
Glock, N., Roy, A.S., Romero, D., Wein, T., Weissenbach, J., Revsbech, N.P., Dagan, T., 2019. Metabolic preference of nitrate over oxygen as an electron acceptor in foraminifera from the Peruvian oxygen minimum zone. Proc. Natl. Acad. Sci. 116 (8), 2860–2865.
Goubert, E., Néraudeau, D., Rouchy, J.M., Lacour, D., 2001. Foraminiferal record of environmental changes: Messinian of the Los Yesos area (Sorbas Basin, SE Spain). Palaeogeography, Palaeoclimatology, Palaeoecology 175 (1–4), 61–78.
Guibourdenche, L., Cartigny, P., Dela Pierre, F., Natalicchio, M., Aloisi, G., 2022. Cryptic sulfur cycling during the formation of giant gypsum deposits. Earth Planet. Sci. Lett. 593, 117676.
Hemleben, C., Spindler, M., Anderson, O.R., 1989. Taxonomy and species features. Modern planktonic foraminifera 8–32.
Hsu, K.J., 1972. Origin of saline giants: a critical review after the discovery of the Mediterranean evaporite. Earth Sci. Rev. 8 (4), 371–396.
Irace, A., Dela Pierre, F., Clari, P., 2005. Normal and chaotic messinian successions at the North-eastern margin of the Langhe domain, Tertiary Piedmont Basin. Bollettino della Società Geologica Italiana 77–85.
Jorissen, F.J., de Stigter, H.C., Widmark, J.G., 1995. A conceptual model explaining benthic foraminiferal microhabitats. Mar. Micropaleontol. 26 (1–4), 3–15.
Kallel, N., Paterne, M., Labeyrie, L., Duplessy, J.C., Arnold, M., 1997. Temperature and salinity records of the Tyrrhenian Sea during the last 18,000 years. Palaeogeography, Palaeoclimatology, Palaeoecology 135 (1–4), 97–108.
Kontakiotis, G., Butiseacă, G.A., Antonarakou, A., Agiadi, K., Zarkogiannis, S.D., Krsnik, E., Vasiliev, I., 2022. Hypersalinity accompanies tectonic restriction in the eastern Mediterranean prior to the Messinian Salinity Crisis. Palaeogeography, Palaeoclimatology, Palaeoecology 592, 110903.
Kouwenhoven, T.V., Van der Zwaan, G.J., 2006. A reconstruction of late Miocene Mediterranean circulation patterns using benthic foraminifera. Palaeogeography, Palaeoclimatology, Palaeoecology 238 (1–4), 373–385.
Krijgsman, W., Fortuin, A.R., Hilgen, F.J., Sierro, F.J., 2001. Astrochronology for the Messinian Sorbas basin (SE Spain) and orbital (precessional) forcing for evaporite cyclicity. Sediment. Geol. 140 (1–2), 43–60.
Landini, W., Sorbini, L., 1989. Ichthyofauna of the evaporitic Messinian in the Romagna and Marche regions. Bollettino della Società Paleontologica Italiana 28, 287–293.
Laskar, J., Robutel, P., Joutel, F., Gastineau, M., Correia, A.C., Levrard, B., 2004. A long-term numerical solution for the insolation quantities of the Earth. Astron. Astrophys. 428 (1), 261–285.
Lozar, F., Negri, A., 2019. A review of basin-wide calcareous nannofossil bioevents in the Mediterranean at the onset of the Messinian salinity crisis. Marine Micropaleontology 151, 101752.
Lozar, F., Violanti, D., Dela Pierre, F., Bernardi, E., Cavagna, S., Clari, P., Trenkwalder, S., 2010. Calcareous nannofossils and foraminifers herald the Messinian salinity crisis: the Pollenzo section (Alba, Cuneo; NW Italy). Geobios 43 (1), 21–32.
Lozar, F., Violanti, D., Bernardi, E., Dela Pierre, F., Natalicchio, M., 2018. Identifying the onset of the Messinian salinity crisis: a reassessment of the biochronostratigraphic tools (Piedmont Basin, NW Italy). Newsletters on Stratigraphy 51 (1), 11–31.
Mancini, A.M., Gennari, R., Ziveri, P., Mortyn, P.G., Stolwijk, D.J., Lozar, F., 2020. Calcareous nannofossil and foraminiferal trace element records in the Sorbas Basin: a new piece of the Messinian Salinity Crisis onset puzzle. Palaeogeography, Palaeoclimatology, Palaeoecology 554, 109796.
Lugli, S., Manzi, V., Roveri, M., Schreiber, C.B., 2010. The primary lower gypsum in the Mediterranean: a new facies interpretation for the first stage of the Messinian salinity crisis. Palaeogeogr. Palaeoclimatol. Palaeoecol. 297 (1), 83–99.
Mancini, A.M., Gennari, R., Natalicchio, M., Dela Pierre, F., Carnevale, G., Pastero, L., Lozar, F., 2022. Taphonomic bias on calcareous micro and nannofossils and paleoenvironmental evolution across the Messinian Salinity Crisis onset: Insights from the Sorbas Basin (SE Spain). Palaeogeography, Palaeoclimatology, Palaeoecology 599, 111056.
Manzi, V., Gennari, R., Hilgen, F., Krijgsman, W., Lugli, S., Roveri, M., Sierro, F.J., 2013. Age refinement of the Messinian salinity crisis onset in the Mediterranean. Terra Nova 25 (4), 315–322.
Martínez-Botí, M.A., Mortyn, P.G., Schmidt, D.N., Vance, D., Field, D.B., 2011. Mg/ca in foraminifera from plankton tows: Evaluation of proxy controls and comparison with core tops. Earth Planet. Sci. Lett. 307 (1–2), 113–125.
McCorkle, D.C., Emerson, S.R., Quay, P.D., 1985. Stable carbon isotopes in marine porewaters. Earth Planet. Sci. Lett. 74 (1), 13–26.
Mejía-Molina, A., Flores, J.A., Torres Torres, V., Javier Sierro, F., 2010. Distribution of calcareous nannofossils in Upper Eocene-Upper Miocene deposits from Northern Colombia and the Caribbean Sea. Rev. Esp. Micropaleontol. 42 (3), 279.
Moissette, P., Cornée, J.J., Antonarakou, A., Kontakiotis, G., Drinia, H., Koskeridou, E., Karakitsios, V., 2018. Palaeoenvironmental changes at the Tortonian/Messinian boundary: a deep-sea sedimentary record of the eastern Mediterranean Sea. Palaeogeography, Palaeoclimatology, Palaeoecology 505, 217–233.
Munnecke, A., Samtleben, C., 1996. The formation of micritic limestones and the development of limestone-marl alternations in the Silurian of Gotland, Sweden. Facies 34, 159–176.
Munnecke, A., Wright, V.P., Nohl, T., 2023. The origins and transformation of carbonate mud during early marine burial diagenesis and the fate of aragonite: a stratigraphic sedimentological perspective. Earth-Science Reviews 239, 104366.
Murray, J.W., 2006. Ecology and Applications of Benthic Foraminifera. Cambridge university press.

Natalicchio, M., Dela Pierre, F., Lugli, S., Lowenstein, T.K., Feiner, S.J., Ferrando, S., Clari, P., 2014. Did late Miocene (Messinian) gypsum precipitate from evaporated marine brines? Insights from the Piedmont Basin (Italy). Geology 42 (3), 179–182.
Natalicchio, M., Dela Pierre, F., Birgel, D., Brumsack, H., Carnevale, G., Gennari, R., Peckmann, J., 2019. Paleoenvironmental change in a precession-paced succession across the onset of the Messinian salinity crisis: Insight from element geochemistry and molecular fossils. Palaeogeography, Palaeoclimatology, Palaeoecology 518, 45–61.
Natalicchio, M., Pellegrino, L., Clari, P., Pastero, L., Dela Pierre, F., 2021. Gypsum lithofacies and stratigraphic architecture of a Messinian marginal basin (Piedmont Basin, NW Italy). Sedimentary Geology 425, 106009.
Néraudeau, D., Videt, B., Courville, P., Goubert, E., Rouchy, J.M., 2002. Corrélation des niveaux fossilifères marins interstratifiés dans les gypses messiniens, entre la carrière de Los Yesos et la carrière de Molinos de Aguas (bassin de Sorbas, SE Espagne). Geodiversitas 24 (3), 659–667.
Pellegrino, L., Natalicchio, M., Abe, K., Jordan, R.W., Longo, S.E.F., Ferrando, S., Dela Pierre, F., 2021. Tiny, glassy, and rapidly trapped: the nano-sized planktic diatoms in Messinian (late Miocene) gypsum. Geology 49 (11), 1369–1374.
Perch-Nielsen, K., 1985. Cenozoic calcareous nannofossils. Plankton stratigraphy 427–455.
Pilade, F., Vasiliev, I., Birgel, D., Dela Pierre, F., Natalicchio, M., Mancini, A., Gennari, R., 2023. Deciphering the termination of the Messinian salinity crisis: the alkenone record of the Miocene-Pliocene transition in the northern Mediterranean. Palaeogeography, Palaeoclimatology, Palaeoecology 631, 111831.
Polyak, L., Stanovoy, V., Lubinski, D.J., 2003. Stable isotopes in benthic foraminiferal calcite from a river-influenced Arctic marine environment, Kara and Pechora Seas. Paleoceanography 18 (1).
Popov, S.V., Shcherba, I.G., Ilyina, L.B., Nevesskaya, L.A., Paramonova, N.P., Khondkarian, S.O., Magyar, I., 2006. Late Miocene to Pliocene palaeogeography of the Paratethys and its relation to the Mediterranean. Palaeogeography, Palaeoclimatology, Palaeoecology 238 (1–4), 91–106.
Pujol, C., Grazzini, C.V., 1995. Distribution patterns of live planktic foraminifers as related to regional hydrography and productive systems of the Mediterranean Sea. Marine Micropaleontology 25 (2–3), 187–217.
Reghizzi, M., Gennari, R., Douville, E., Lugli, S., Manzi, V., Montagna, P., et al., 2017. Isotope stratigraphy (87Sr/86Sr, δ18O, δ13C) of the Sorbas basin (Betic Cordillera, Spain): Paleoceanographic evolution across the onset of the Messinian salinity crisis. Palaeogeography, Palaeoclimatology, Palaeoecology 469, 60–73.
Rohling, E.J., Schiebel, R., Siddall, M., 2008. Controls on Messinian lower evaporite cycles in the Mediterranean. Earth Planet. Sci. Lett. 275 (1–2), 165–171.
Rouchy, J.M., Caruso, A., 2006. The Messinian salinity crisis in the Mediterranean basin: a reassessment of the data and an integrated scenario. Sedimentary Geology 188, 35–67.
Roveri, M., Flecker, R., Krijgsman, W., Lofi, J., Lugli, S., Manzi, V., Stoica, M., 2014. The Messinian Salinity Crisis: past and future of a great challenge for marine sciences. Mar. Geol. 352, 25–58.
Roveri, M., Lugli, S., Manzi, V., 2024. The Desiccation and Catastrophic Refilling of the Mediterranean: 50 years of Facts, Hypotheses, and Myths around the Messinian Salinity Crisis. Ann. Rev. Mar. Sci. 17.
Ruggieri, G., 1967. The Miocene and later evolution of the Mediterranean Sea. Aspects of Tethyan biogeography 7, 283–290.
Sabino, M., Schefuß, E., Natalicchio, M., Dela Pierre, F., Birgel, D., Bortels, D., Peckmann, J., 2020a. Climatic and hydrologic variability in the northern Mediterranean across the onset of the Messinian salinity crisis. Palaeogeography, Palaeoclimatology, Palaeoecology 545, 109632.
Sabino, M., Pierre, F.D., Natalicchio, M., Birgel, D., Gier, S., Peckmann, J., 2020b. The response of water column and sedimentary environments to the advent of the Messinian salinity crisis: insights from an onshore deep-water section (Govone, NW Italy). Geol. Mag. 158 (5), 825–841.
Sabino, M., Birgel, D., Natalicchio, M., Dela Pierre, F., Peckmann, J., 2021. Carbon isotope excursions during the late Miocene recorded by lipids of marine Thaumarchaeota, Piedmont Basin. Geology 50 (1), 32–36.
Saint Martin, J.P., Pestrea, S., Conesa, G., 2001. Les assemblages de diatomées des niveaux infra-gypseux du bassin messinien de Sorbas (Espagne). Cryptogam. Algol. 22 (1), 127–149.
Schiebel, R., Hemleben, C., 2017. Planktic Foraminifers in the Modern Ocean, vol. 358. Springer, Berlin.
Schmiedl, G., Pfeilsticker, M., Hemleben, C., & Mackensen, A. (2004). Environmental and biological effects on the stable isotope composition of recent deep-sea benthic foraminifera from the western Mediterranean Sea. Marine Micropaleontology, 51 (1–2), 129–152.
Selli, R., 1960. Il Messiniano MAYER-EYMAR 1867: proposta di un neostratotipo. Museo Geologico "Giovanni Capellini".
Sierro, F.J., Flores, J.A., Francés, G., Vazquez, A., Utrilla, R., Zamarreño, I., Barcena, M. A., 2003. Orbitally-controlled oscillations in planktic communities and cyclic changes in western Mediterranean hydrography during the Messinian. Palaeogeography, Palaeoclimatology, Palaeoecology 190, 289–316.
Sturani, C., 1973. A fossil eel (Anguilla sp.) from the Messinian of Alba (Tertiary Piedmontese Basin). Palaeoenvironmental and palaeogeographic implications. In: Messinian Events in the Mediterranean, vol. 7, pp. 243–255. North-Holland Amsterdam.
Sturani, C., Sampò, M., 1973. Il Messiniano inferiore in facies diatomitica nel Bacino Terziario Piemontese. Mem. Soc. Geol. Ital. 12, 335–358.
Tzevahirtzian, A., Caruso, A., Andreetto, F., Bonomo, S., Krijgsman, W., 2023. A bio-chronostratigraphic study of the upper Miocene from the northern Caltanissetta Basin, Sicily (core 3AGN2S04). Implications for dating the Messinian Salinity Crisis onset. Sedimentary Geology 445, 106330.
Van der Laan, E., Gaboardi, S., Hilgen, F.J., Lourens, L.J., 2005. Regional climate and glacial control on high-resolution oxygen isotope records from Ain el Beida (latest Miocene, Northwest Morocco): a cyclostratigraphic analysis in the depth and time domain. Paleoceanography 20 (1).
Vasiliev, I., Karakitsios, V., Bouloubassi, I., Agiadi, K., Kontakiotis, G., Antonarakou, A., et al., 2019. Large sea surface temperature, salinity, and productivity-preservation changes preceding the onset of the Messinian Salinity Crisis in the eastern Mediterranean Sea. Paleoceanography and Paleoclimatology 34 (2), 182–202.
Violanti, D., Lozar, F., Natalicchio, M., Dela Pierre, F., Bernardi, E., Clari, P., Cavagna, S., 2013. Stress-tolerant microfossils of a Messinian succession from the Northern Mediterranean basin (Pollenzo section, Piedmont, northwestern Italy). Bollettino della Società Paleontologica Italiana 52 (1), 46.
Wheeley, J.R., Cherns, L., Wright, V.P., 2008. Taphonomic windows and molluscan preservation. Palaeogeogr. Palaeoclimatol. Palaeoecol. 270 (3–4), 220–229.
Zachariasse, W.J., Lourens, L.J., 2022. The Messinian on Gavdos (Greece) and the status of currently used ages for the onset of the MSC and gypsum precipitation. Newsl. Stratigr. 55 (3), 333–360.
Ziveri, P., Baumann, K.H., Bockel, B., Bollmann, J., Young, J., 2004. Present day coccolithophore-biogeography in the Atlantic Ocean. In: Coccolithophores: From Molecular Processes to Global Impact. Springer Verlag, pp. 403–428.
Zonneveld, K.A., Pospelova, V., 2015. A determination key for modern dinoflagellate cysts. Palynology 39 (3), 387–409.